Journal of Molecular Structure 1250 (2022) 131712

Contents lists available at ScienceDirect

Journal of Molecular Structure

journal homepage: www.elsevier.com/locate/molstr

Green synthesis and mechanism analysis of a new metal-organic framework constructed from Al (III) and 3,4-dihydroxycinnamic acid extracted from *Satureja hortensis* and its anticancerous activities

Malihe Zeraati[a], Vali Alizadeh[b], Supat Chupradit[c], Narendra Pal Singh Chauhan[d,**], Ghasem Sargazi[e,*]

[a] Department of Materials Engineering, Shahid Bahonar University of Kerman, 761694111 Kerman, Iran
[b] Department of Petroleum, Faculty of Engineering, University of Garmsar, Garmsar, Iran
[c] Department of Occupational Therapy, Faculty of Associated Medical Sciences, Chiang Mai University, Chiang Mai 50200, Thailand
[d] Department of Chemistry, Faculty of Science, Bhupal Nobles' University, Udaipur-313002 Rajasthan, India
[e] Noncommunicable Diseases Research Center, Bam University of Medical Sciences, Bam, Iran

ARTICLE INFO

Article history:
Received 5 December 2020
Revised 9 October 2021
Accepted 11 October 2021
Available online 13 October 2021

Keywords:
Al-mof
Sustainable
Extract
Characterization
Anticancer

ABSTRACT

In this study, aluminium nitrate and a carboxylate linker extracted from *Satureja hortensis* were used to develop a sustainable aluminium-based metal-organic framework (Al-MOF). Al-MOF has been extensively characterized using FT-IR and Raman spectroscopy, XRD, TEM, FE-SEM, TG-DTA, and Brunauer – Emmett – Teller (BET) techniques. The prepared samples, which included large hexagons and triangular channels, had a pore size of about 20 nm and a surface area of about 1245.2 m^2/g, according to the results. The mechanism of the formation of Al-MOF has been proposed based on density functional theory with B3LYP and 6–31 G (d,p) as the basis set. The highest occupied molecular orbits (HOMO) to the lowest unusable molecular orbit (LUMO) are also used to discuss chemical reactivity patterns in molecules. Al-MOF has demonstrated anticancer activity against human breast cancer (MDA-MB-468) cell lines, suggesting that it could be a promising anticancer drug for clinical use.

1. Introduction

Metal-organic frameworks (MOFs) are appealing organic-inorganic composites composed of metal clusters (e.g., Zr, Zn, Cr, Cu, and Al) and organic linkers (e.g. aromatic carboxylic acids) [1]. Unique ability to regulate the structure at different ligands and metal centers due to the evolution of MOFs as a good candidate for various utilities including, fluorescence [2], heat transformation [3], separation [4], catalysis [5], sensor [6], gas storage [7] and sensing [8]. According to the literature, applications of MOFs with lightweight structures, high stability, and low harmful potential are hot topics for many different types of research [9]. Light metals such as alkali Mg, Ca and Al were therefore considered to be the metal base [10]. aluminium (Al) has unique physical and chemical properties and is abundant in the Earth's crust, making it a good candidate for many engineering applications, such as the interconnection of octahedral to form several inorganic sub-networks that provide multi-dimensional [10,11]. Furthermore, Al is one of the most abundant metals, with non-toxic salts that are simple to use and inexpensive [12]. Unique specification of Al, such as the stability of Al in aqueous solutions such as Al^{3+} and Al^{2+}, have led to the evolution of Al as a good candidate for the preparation of aluminium MOFs (Al-MOFs) as attractive substances for advanced materials [13].

Various approaches to the preparation of Al-MOFs include hydrothermal [14], solvothermal [15], sol-gel [16] and slow diffusion techniques [17]. The main disadvantage of this approach is the use of hazardous materials, particularly organic precursors. Typically, dimethylformamide (DMF) [18] is the most common organic linker and contains hazardous chemical compounds from the aspect of handling and disposal [19]. As a result, the use of green sources as a link precursor can be regarded as a revolution in MOF preparation. Ionic liquids, natural oils, and plant extracts are examples of such sources, all of which have a high level of acceptability in terms of green technology [20]. Green MOF synthesis also reduces or eliminates the need for organic solvents, operates at low temperatures and pressures, and requires less time to react. These benefits have increased the efficiency of the green technique [21]. Numerous studies have been conducted on the effects of nano-Al and

* Corresponding author.
** Co-corresponding author.
E-mail addresses: narendrapalsingh14@gmail.com (N.P.S. Chauhan), g.sargazi@gmail.com (G. Sargazi).

https://doi.org/10.1016/j.molstruc.2021.131712
0022-2860/

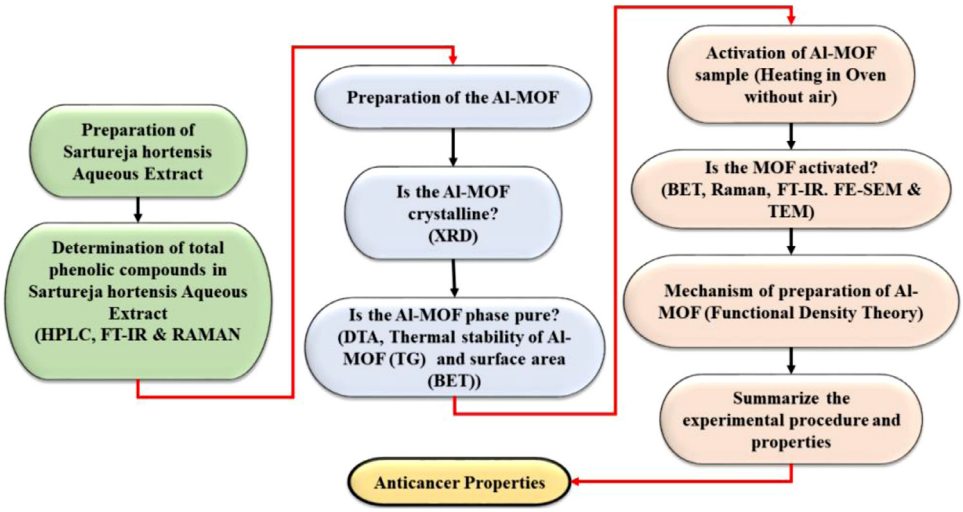

Fig. 1. The flowchart of synthesis of Al-MOF in present study.

its various compounds [22]. Muehlmann and Sun et al., for example, demonstrated that aluminium oxide nanoparticles as drug carriers are promising for photodynamic cancer therapy as well as for the activation of the immune system in cancer diseases [23]. Wang et al. revealed the use of aluminium anode nanotubes as a carrier of anticancer drugs is shown on the MDA cancer cell line. Protein from the family of tumour necrosis factors that induce apoptosis was used as a model drug. Anodic alumina nanotubes that have been structurally engineered can be used as nano-carriers for the delivery of anticancer therapeutics [24]. So, the oxidation of aluminium and copper has anticancer and antimicrobial properties due to its highly porous structure.

Satureja hortensis (*S. hortensis*) is a native plant of North America, western and southern Asia (including Iran) and southern Europe. *S. hortensis* including a variety of chemical compositions, in particular 3,4-dihydroxycinnamic acid (Caffeic acid), 3,4,5-trihydroxybenzoic acid (gallic acid), 3-O-Caffeoylquinic acid (chlorogenic acid) and 4–hydroxy-3-methoxycinnamic acid (ferulic acid) [25]. In traditional medicine, it is used to treat diarrhoea, indigestion, nausea, muscle aches, and cramps [26]. Its species has caused the wide application of *S. hortensis* in traditional medicines due to its inherent antioxidant, antibacterial and antifungal properties [27]. According to Markham method [28], phenolic compounds obtained from aqueous extract of *S. hortensis* are ferulic acid, gallic acid, trans-cinnamic acid, 2-hydroxycinamic acid, quercetin, caffeic acid, chlorogenic acid, kaempferol and *p*-coumaric acid [29].

To the best of our knowledge, no reports of Al-MOF preparation using plant extract as an organic precursor have been reported. In this study, we attempted to extract 3,4-dihydroxycinnamic acid from *S. hortensis* and use it as a precursor in the organic binder for the preparation of Al-MOF. The flowchart of Al-MOF synthesis is depicted in Fig. 1.

Accordingly, the main contribution of the current study can be categorized as following:

1. Water is used as a solvent at a relatively low temperature (80 °C) and for a short period of time (60 min).
2. S. hortensis extract was used to extract 3,4-dihydroxycinnamic acid.
3. Green Al-MOF production using aluminium nitrate as a precursor to Al and 3,4-dihydroxycinnamic acid as a precursor to organic linker.
4. The Al-MOF prepared has a low activated temperature as well as a low time computed from thermal analysis data.
5. DFT analysis should be used for each mechanism of Al and 3,4-dihydroxycinnamic acid as organic precursors.

FTIR, Raman spectroscopy, XRD, FE-SEM, FTG-DTA, and BET analysis are used to characterize the synthesized Al-MOF.

2. Density functional theory (DFT)

Density functional theory (DFT) (i.e., a ground-state theory used to determine the ground states of a quantum system in order to estimate relevant values, such as ground state energy) is an intriguing and powerful tool [30]. The particle density of a system with interacting N particles is used as the original value in DFT instead of the wave function [31]. Frontier orbital energy gap is the subtraction of the highest occupied molecular orbital (HOMO) to the lowest unoccupied molecular orbit (LUMO). The Frontier orbital energy gap could be used to determine the interaction between different species. Harmonic vibrational waves were calculated using second-order analytical derivatives to confirm the convergence of minimums on the potential surface and to evaluate the zero-vibration contrast energy. As shown in Fig. 2, in the finite-charge regime at one of the metal/molecule interfaces, the role of non-boundary modes is important, as these channels provide additional channels through which they can be used. An interface can be used to transmit the load [32]. As a result, the VESTA software used HOMO-LUMO to determine the most likely mechanism of Al-MOF formation [33]. Using the Gauss-09 quantum chemistry package, kinetic and thermochemical data were estimated at the theoretical DFT level [34]. Since absolute values of the enthalpy and Gibbs free energy of the molecule can be obtained by theoretical calculation, the enthalpy of the reaction and the Gibbs energy of each possible reaction are obtained by using these energy values [35].

The CA ineludible C=C, C–H, H–O, and C–O bonds must be taken into account during the interaction with the aluminium precursor. The optimization of appropriate molecules was carried out using the B3LYP theory by the 6–31 G set [15]. Gaussian 09 was used to make the estimates [36]. All optimized structures of *S. hortensis* were confirmed to have minimal energy compatibility.

3. Experimental

S. hortensis aqueous extract and aluminium chloride [$AlCl_3{\cdot}6H_2O$] extracts are used to obtain 3,4-dihydroxycinnamic acid. The reagents that used for the chemical synthesis of Al-MOF

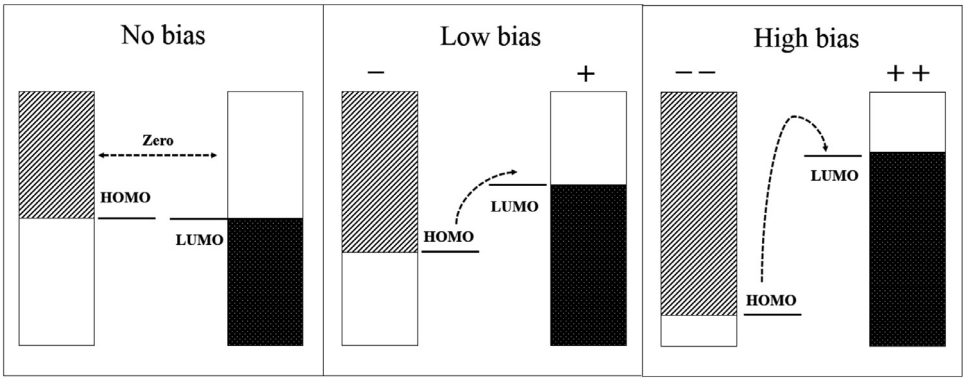

Fig. 2. Proposed charge transfer mechanism HOMO and LUMO [31].

are aluminium nitrate [$Al(NO_3)_3{\cdot}9H_2O$], deionized water and 3,4-dihydroxycinnamic acid, i.e., the green organic linker.

3.1. Preparation of satureja hortensis aqueous extract

To make S. hortensis aqueous extract, first place 30 g of dry Satureja cut (harvested from Golboft in Kerman province of Iran, 2018) in clevenger-type apparatus with 300 mL of distilled water for 45 min, then cool and filter three times with centrifugal spinning machine at 4000 rpm [37]. The extract was kept in refrigerator for future uses.

3.2. Separation of 3,4-Dihydroxycinnamic acid in aqueous extract of satureja hortensis

The Markham method has been used to extract flavonoids [28]. Primarily, 250 mL of 2% $AlCl_3{\cdot}6H_2O$ solution mixed with 40 mL *S. hortensis* aqueous extract. After storage for 15 min at room temperature, The absorbence response was measured at 430 nm.

3.3. Green synthesis of AL-MOF

The synthesis process was carried out in ambient atmosphere. Firstly, about 3.3 g of Al precursor, i.e., $Al(NO_3)_3{\cdot}9H_2O$, was dissolved at 12.5 mL deionized water as the solvent at 80 °C. Approximately 3.3 g of 3, 4-dihydroxycinnamic acid was added to the Al solution at the stirring rate of 300 rpm. The transparent colloidal of the initial solution turns light-yellow during this step. After 60 min of synthesis, a white precipitate is formed from the original yellow solution. This white precipitate has been collected and dried. Finally, taking into account the thermal analysis results, the prepared sample was kept in a vacuum oven at 120 °C for 5 min in order to activate its structure. XRD analysis was carried out at 25 °C using a Phillips diffractometer with a copper anode and a graphite monochromatic for the selection of Cu-kα radiation (λ = 1.541 Å) for the assessment of the crystalline size and the phase analysis of the prepared sample. The Nanosem-450 model was used to investigate the morphology and size of the prepared particles.

3.4. Characterization

Field-emission scanning electron microscope (FE-SEM) images were acquired by an Inspect F scanning electron microscope operating at 3 kV and equipped with an energy dispersive X-ray (EDX) spectroscopy and a transmission electron microscopy (TEM). FT-IR spectra of the samples were measured on a Varian LS chemical imaging microscope at 4000–400 cm^{-1}. Raman spectral lines were obtained in a Raman microscope spectrometer within RENISHAW with the 633 nm from He-Ne a laser source. TG/DTA experiments were performed using the TGA /SDTA Q600 system. The samples were heated upto 700 °C at the rate of 10 °C/min. The Brunauer–Emmett–Teller (BET) model used the nitrogen adsorption/desorption isotherms (at the temperature of 196 °C) after the separation at 200 °C and 10–5 mm Hg for at least 4 h to estimate surface-specific regions. The mesoporous size distribution and total mesoporous volume were estimated using the modified Barrett–Joyner–Halenda (BJH) method. GC–MS analysis was also performed using a Thermoquest-Finigan gas chromatograph (equipped with a DB-1 column silica capillary column (60 m * 0.25 mm i.d.; film thickness = 0.25 µm) with four polarization of TRACE mass. Helium tracer was employed as a carrier gas with an ionization voltage equal to 70 eV. The ion source and interface temperatures were 200 °C and 250 °C, respectively. The chromatographic separation for phenolic compounds was achieved using an Agilent 1100 (Agilent Technologies, USA) HPLC system with a binary pump and diode array detector - DAD. The phenolic acids were separated on a ZORBAX SB-Aq (5 µm particle size: 4.6 mm × 250 mm, Agilent) column. The aqueous extract was filtered through 0.45- µm syringe filters and directly injected through a 30 µL fixed loop onto the column. Solvents used were of chromatography grade and were obtained from J. T. Baker (Deventer, The Netherlands). Ferulic acid (99.0%), *trans*-cinnamic acid (99.0%), 3,4,5-trihydroxybenzoic acid (99.9%), 3,4-dihydroxycinnamic acid (98.0%), 2-hydroxycinamic acid (97.0%), *p*-coumaric acid (98.0%), chlorogenic acid (95.0%), quercetin (98.0%) and kaempferol (97.0%), all Sigma–Aldrich, were used as analytical standards. The stock standard solutions were prepared by dissolving the required analytical standard in methanol, while the working solution, *i.e.*, the mixture of the studied phenol compounds, was obtained by mixing and diluting the stock standards with mobile phase, resulting in a final mass concentration of 100 µg mL^{-1}. The composite mixtures of all phenol compounds at appropriate concentrations were used to spike samples in the data validation settings. Acetic acid was pure analytical grade (Carl Roth).

4. Results and discussion

The main constituent of phenol components was 3,4-dihydroxycinnamic acid (80.27 µg/ g). The second largest component was 3,4,5-trihydroxybenzoic acid (13.16 µg/ g). Quercetin, *p*-coumaric acid, chlorogenic acid and ferulic acid were reported at concentrationss of 2.26, 1.69, 1.46 and 0.48 µg /g, respectively.

Fig. 4 shows the FT-IR spectrum of *S. hortensis* extract. Extensive and intense absorption in the range 3700–3000 cm^{-1} is attributed to the tensile vibrations of O–H bands of water and other carbohydrates. These absorbers are highly overlapping and displayed by

Table 1
Step by step comparison of activation temperature and time other methods to the synthesis Al-MOFs.

Ref/ Year	Precursor	Linker	Method	Activities-temperature (°C)	Time (h)
[41]/ 2010	$Al(NO_3)_3{\cdot}9H_2O$	1,4-benzenedicarboxylic acid	Hydrothermal	330	72
[42]/ 2013	$AlCl_3$ and $Al(NO_3)_3{\cdot}9H_2O$	Acetic acid and DFM	Solvothermal	150	24
[43]/ 2013	$Al(NO_3)_3{\cdot}9H_2O$	Terephthalic acid	Hydrothermal	330	72
[44]/ 2014	$AlCl_3{\cdot}6H_2O$	2-aminoterephthalic acid	Hydrothermal	15	5
[45]/ 2016	$Al_2(SO_4)_3{\cdot}18H_2O$	Adipic acid	Solvothermal	130	12
[46]/ 2018	$Al(NO_3)_3{\cdot}9H_2O$	Trimesic acid	Hydrothermal	180	24
[47]/ 2018	$Al(NO_3)_3{\cdot}9H_2O$	DMF and DI water	Solvothermal	90	120
This work	$Al(NO_3)_3{\cdot}9H_2O$	3,4-Dihydroxycinnamic Acid	Sol-Gel	120	5 min

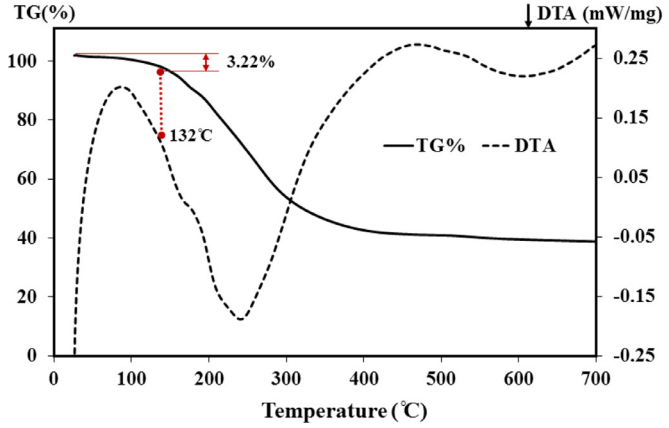

Fig. 3. The DTA/TGA analysis of the synthesized Al-MOF.

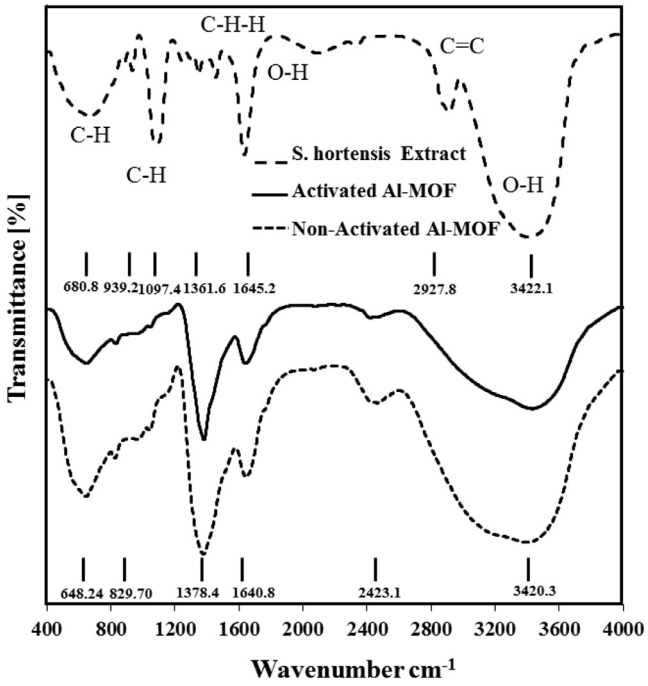

Fig. 4. The comparison of *S. hortensis* extract, non- activated and activated Al-MOF.

broadband. Also, the H–O-H bending or water absorption band in 1645 cm^{-1} related to the preparation of extract in water. The C–H or carbohydrate stretches are also found at the range of 3000-2700 cm^{-1}. A number of absorption bands corresponding to the C–C-H deformation vibrations of glucose and fructose are shown in the spectral range between 1500 and 750 cm^{-1}.

The process of "activating" or removing solvents or other guest chemicals in the MOF must be carried out after the preparation of MOF. The key role in activation is that the main structure of the MOF must be constant [38]. Robertson et al. have explored the importance of activation for modification of MOF structure [39]. It was worth noting that, by using high temperatures through activation, the prepared MOF framework may deteriorate. Thermal-calorimetry analysis must therefore be used to determine the temperature of the activation [40]. Activated temperatures of some Al-MOFs have been reported in Table 1. We therefore use green solvents that contain many organic compounds that are removed from the sample for a short time due to their volatility.

According to the literature [38], activation of Al-MOF effectively enhanced the performance of the prepared sample. Structural water removal can be considered as a viable method for different types of MOF activation. Thermal analysis was used to determine the appropriate temperature for the activation of Al-MOF [47]. Fig. 3 shows the results of TG/DTA analysis for prepared sample. In first stage of degradation, the weight loss (3.22%) initiated at the temperature range between 100 °C and continued to 132 °C. In this regard, the activation temperature was selected to be equal to 120 °C for 5 min. FT-IR analysis is used to ensure the accuracy of activation for the removal of water from the prepared sample (Fig. 4). The second region is the disappearance at 200–300 °C, which can be caused by the breakdown of the framework, e.g. the breakdown of the 3,4-dihydroxycinnamic acid ligands. The third region is the casualty at 400–500 °C after which the residual mass was no more than 38% of original mass. This weight loss reflects the removal of aromatic rings from covalent bonds of the framework [47,48]. As shown, a temperature increase of up to 600 °C causes a weight loss that would remove the OH groups [46,49].

Fig. 4 illustrated the FT-IR of samples including, non-activated and activated form of prepared Al-MOF. Peaks appeared at 648 cm^{-1} and 829 cm^{-1} is attributed to C–H bending vibrations present in CH_2 groups whereas a strong peak appeared at 1378 cm^{-1} is due to C–H bending vibrations present in CH_3 groups [50]. Peaks appeared at 2423 and 1640 cm^{-1} is attributed to C=C stretching vibrations. It should be noted that the peak appeared at 3420 cm^{-1} strongly suggested the formation of Al-MOF [51]. An intense and broad peak appeared ranging from 3700 to 3000 cm^{-1} is attributed to O–H stretching vibrations due to bound water present in carbohydrates. Also, a peak appeared at 1640 cm^{-1} is attributed to O–H bending vibrations present in water.

The decreased trend of O–H bond after activation is clearly revealed from the FT-IR spectra of non-activated and activated Al-MOF samples. The highlight of the FT-IR spectra for activated and deactivated Al-MOF, by removing excess water, at 3420 cm^{-1} due to O–H stretching vibrations is quite consistent with the proposed structure of final product.

The Raman spectra of the non-activated and activated Al-MOF are shown in Fig. 5. The extreme peak in 1604 cm^{-1} is related to the C=O stretching vibrations present in carboxylate group adjacent to the arranged carbon skeleton such as C–CH, which usually

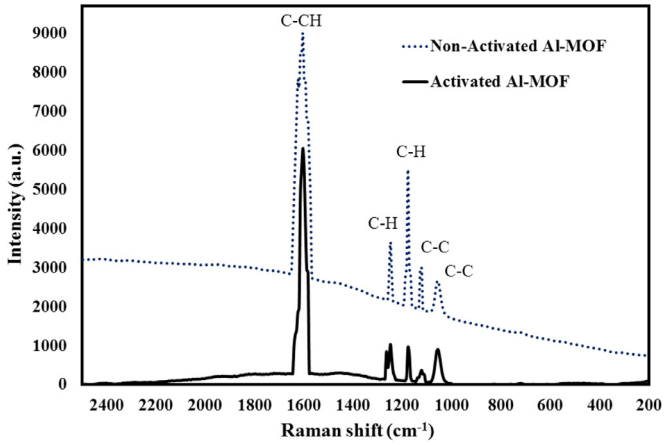

Fig. 5. The Raman spectra of the non- activated, and activated Al-MOF.

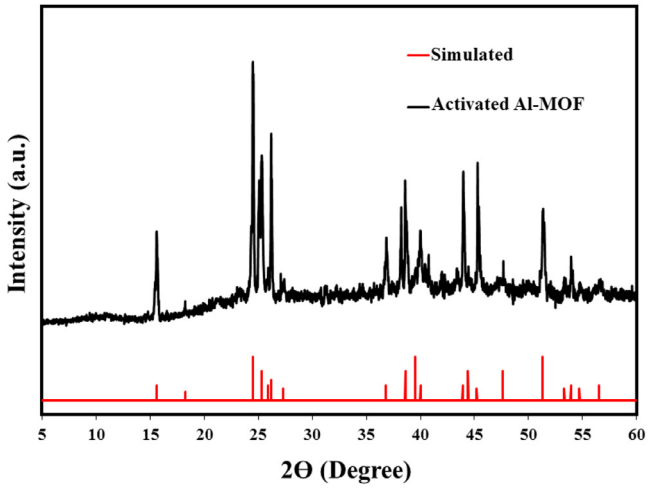

Fig. 6. Comparison of XRD spectra of activated Al-MOF for 60 min at 120 °C and simulated file by Volkringer and coworkers [54].

appears between the 1580 cm^{-1} and 1610 cm^{-1}. The vibrations in the plane of the C–H and C–C bonds of the benzene ring may be the reason for the evolution of the various peaks in the range of 1345 cm^{-1} to 1150 cm^{-1} [52]. By comparing non-activated and activated modes, it is possible to conclude that activation is performed efficiently and without causing damage to the frameworks; activation does not result in the removal of organic matter from the pores.

MOFs are organic frameworks with metallic knots, it was discovered (Al in this study).The exact XRD pattern of these structures should include Al-C-O–H compounds, as a result from which the prepared structure is simulated to MIL-100(Al) [53]. The XRD patterns for this powder are shown in Fig. 6. XRD pattern is in good agreement with a simulated file, and high intensity indicates acceptable crystallinity of the prepared sample using Reference code 96–400–1059 [54]. The final products are therefore of a crystalline nature and confirmed the formation of MIL-100(Al). We can be certain that the MIL-100 is completely degraded based on the FT-IR and Raman spectra results.

To estimate the surface area of the prepared sample used BET analysis (Fig. 7). As shown, the adsorption isotherms of both samples (including non-activated and activated Al-MOFs) are similar to the isotherm IV type and isotherm observation BJH analysis (Fig. 7(b)). The porosity of the activated samples was estimated to be approximately 20 nm, which was replaced by mesoporous

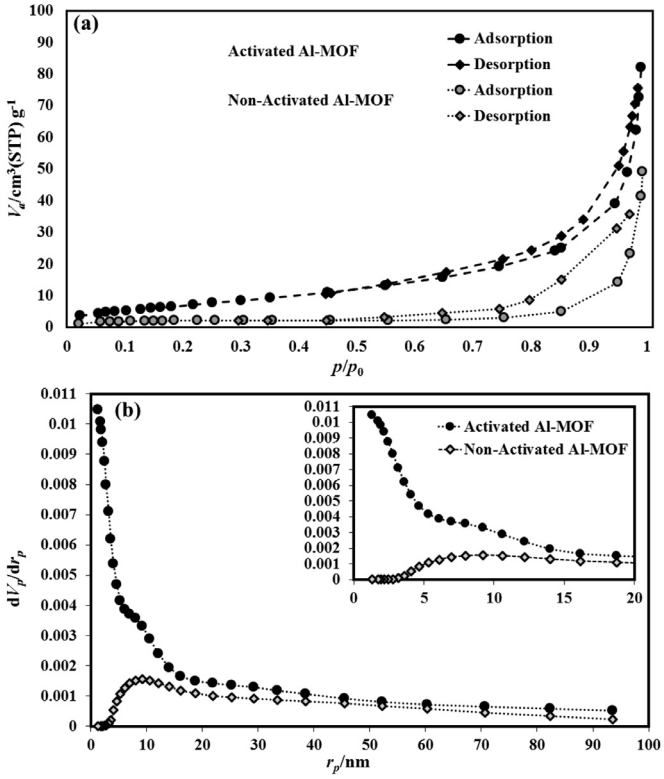

Fig. 7. BET analysis of activated Al-MOF: (a) N_2 adsorption/desorption isotherms and (b) Pore size distribution.

materials [55]. While, the average pore size of activated and non-activated samples was 10.73 m^2/g and 1245.2 m^2/g, respectively. Accordingly, the prepared Al-MOF was accepted as mesoporous martial as reported by Moreno and coworkers [50]. Al-MOF was prepared at 90 °C for 5 days with a surface equal to 30–70 m^2 / g by a combination of DFM / DI water using $Al(NO_3)_3{\cdot}9H_2O$ as precursors. As can be seen (Fig. 7(a)), due to the presence of closed porous in non-activated samples, increasing the pressure of N_2 up to $p/p_0 = 0.3$ dozen effects on the amount of adsorption due to the constraint of diffusion. The activation process can, however, effectively open up the porous and induced higher absorption rate.

The decrease in surface area compared to previous reports is probably due to the presence of organic extract molecules that are not completely removed by activation. In addition, the molecules of solvent trapped in the MOF pores reduce the specific surface area. On the other hand, the Al-MOF powders have been agglomerated and the gas penetration does not occur completely [53,56].

FE-SEM of activated Al-MOF derived from 3,4-dihydroxycinnamic acid an organic linker is shown in Fig. 8a. It can be seen that there is a strong agglomeration of the prepared samples in the layered structure of the administered phenomenon and concluded that layered structure was responsible for the absorption of nitrogen gas. Consideration of elemental distribution in Al-MOFs revealed that the prepared sample is deficient from carbon and may be these parts are enriched with hydroxide compounds (Fig. 8b)).

The spherical geometry of the synthesized sample was confirmed by the TEM image of the Al-MOF mesostructured in Fig. 9. Higher accuracy in TEM image revealed the hollow nature of the prepared structure. The holes diameter is slightly less than 10 nm so that their images correspond to the pore diameter calculated from the nitrogen adsorption isotherm for activated Al-MOF, i.e., about 24 nm. But as is clear, the surface area of prepared sample is higher than the results of BET, which is mainly due to the pores

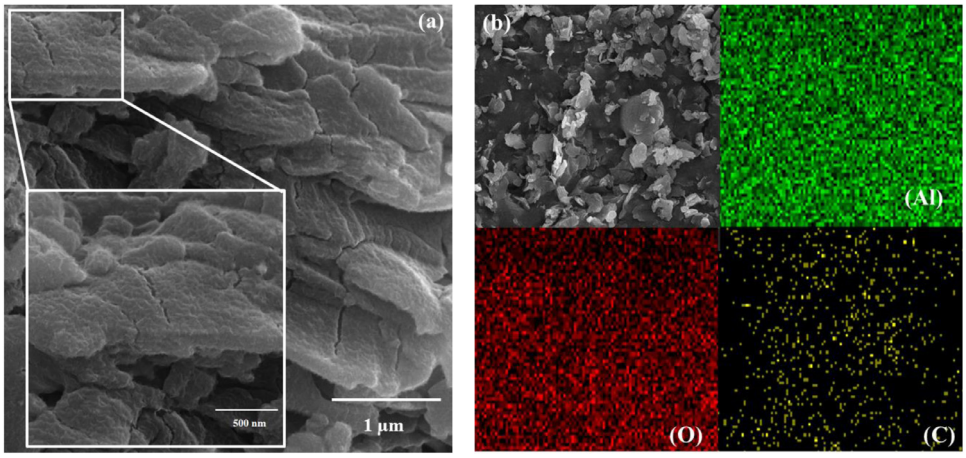

Fig. 8. a) FE-SEM image of activated Al-MOF using 3,4-dihydroxycinnamic acid as an organic linker precursor and b) MAP of elements analysis.

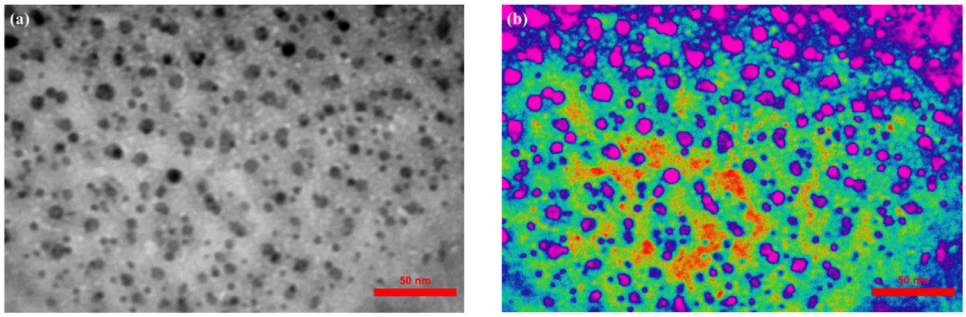

Fig. 9. (a) TEM images of the activated Al-MOF and (b) image analysis of TEM.

being closed as well as multilayer interlocking. By consideration of the surface area as criteria, the fraction of pores (dark area) to the total surface in TEM image was estimated using the image analyser software. As shown in Fig. 9(b), the pink, blue and light blue corresponding to the pore phase, while the background being red and green. These results confirmed the formation of approximately 68% of the pore phase in the prepared sample.

4.1. DFT usage for proposing the mechanism of the formation of AL-MOF

The function density theory (DFT) is used to determine the mechanism of Al-MOF formation. As shown by HPLC, 3,4-dihydroxycinnamic acid (80,27µg/g) is considered to be the most abundant species in the extract. This study used the frontier orbital energy gap as HOMO and LUMO.

Fig. 10(a) showed the structure of orbital energy of $Al(NO_3)_3$ precursors in 353.15 K at 1 atm and Fig. 10(b) illustrated the 3,4-dihydroxycinnamic acid such as organic linker. As shown in Fig. 11, the energy gap of $Al(NO_3)_3$ is 5.93 eV. However, the energy gap of 3.4-dihydroxycinnamic acid is 4.13 eV. The mechanism and reactivity of 3,4-dihydroxycinnamic acid with $Al(NO_3)_3$ precursors is defined as the energy difference of the HOMO precursor $Al(NO_3)_3$ with LUMO acid and the LUMO $Al(NO_3)_3$ with HOMO acid shown in Fig. 11.

Which can be considered the default mechanism of Fig. 12, which is the combination of $Al(NO_3)_3$ and 3,4-dihydroxycinnamic acid organic compound of layers with large cavities, as shown in Fig. 9, the organic and industrial combinations cannot be applied to such a layered structure.

The cytotoxicity of aluminium and Al-MOF was tasted in vitro through MTT assay. As shown in Fig. 13, the MDA-MB-468 cells

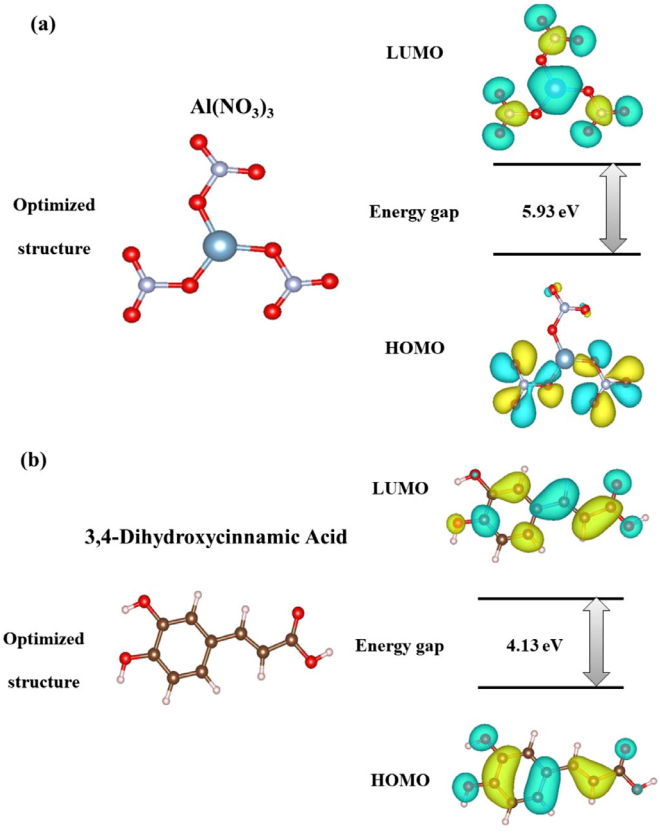

Fig. 10. The optimized structure as HOMO/LUMO, and energy gap of (a) $Al(NO_3)_3$ and (b) 3,4-Dihydroxycinnamic acid.

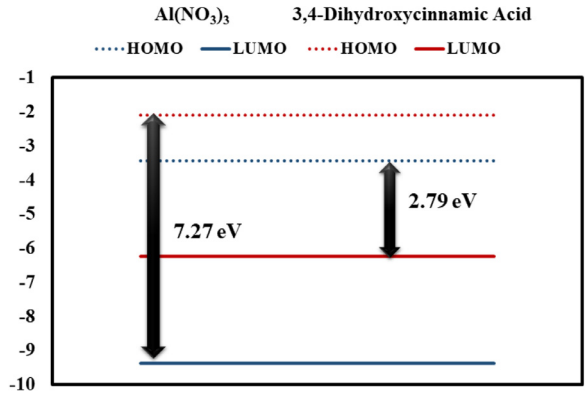

Fig. 11. The HOMO and LUMO energy levels of $Al(NO_3)_3$ and 3,4-Dihydroxycinnamic Acid.

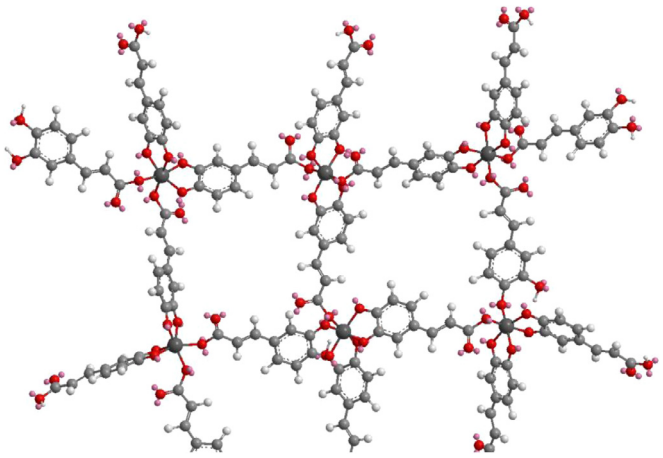

Fig. 12. Proposed structure of Al-MOF.

were treated with different concentrations (0–100 µg/mL) of Al-MOFs. Also, the IC_{50} values (minimum concentration of extract to reduce cell viability to 50%) of extracts of herbs and Al-MOFs after incubation for 24 h and 48 h. The inhibitory effect of the alcoholic extract on cell proliferation was significantly superior to that of aqueous extract. Parallel treatment of the normal cells with these components demonstrated a much less inhibitory effect on the viability of human normal cells. Firstly, up to 100 µg/mL of Al and Al-MOF shown after 24 h and 48 h incubation does not affect the proliferation of MCF10-A cells, i.e., normal cells. The main property of cancer cells is uncontrolled proliferation; so the control of tumour growth is considered to be a valid treatment for cancer therapy [57]. Several studies have shown that the metal-organic frameworks have beneficial aspects, including low cytotoxicity, host-guest interactions, hydrophobic/hydrophilic balance, biodegradability, body distribution, tissue accumulation and excitability, allowing them to be used in biological applications for cancer treatment [58]. Therefore, we have chosen one type of Al-MOFs as a carrier for the anti-proliferative herbal extract. The Al-MOFs seems to be more effective against proliferation of breast cancer cells when compared with herbal extraction. In addition, a low concentration of these bio structures (30 ± 1.2 µM) significantly reduced the growth of MDA-MB-468 cells after 48 h. Thus, Al-MOFs as a safe anticancer agent against the human breast cancer are a potent component to be explored further for its cytotoxic properties.

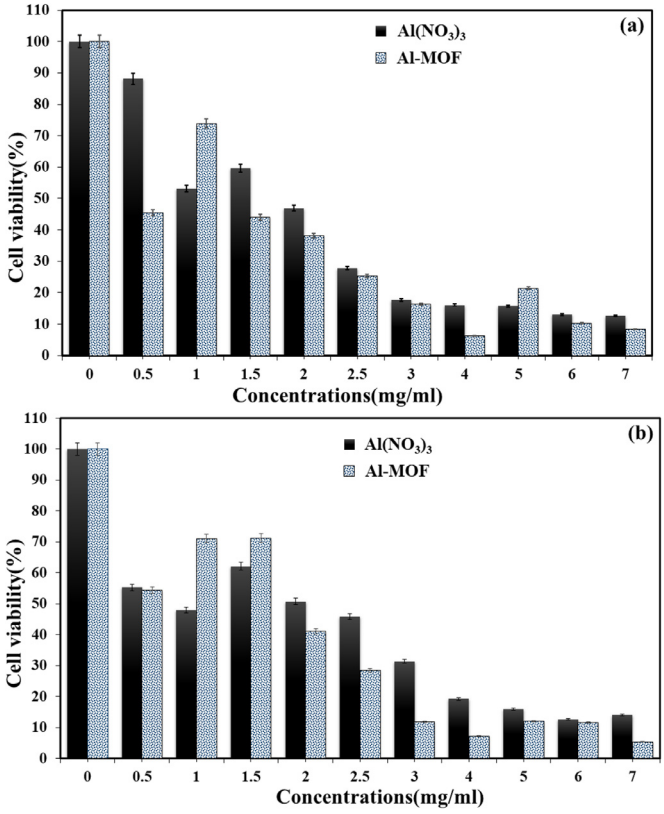

Fig. 13. Cytotoxicity of various concentrations of herbal extraction and A1-MOF (0–100 µM) against human breast cancer cells after incubation for 24 and 48 h (a,b).

5. Conclusions

S. hortensis extract contains aromatic acids such as 3,4-dihydroxycinnamic acid, 3,4,5-trihydroxybenzoic acid, quercetin, p-coumaric acid, chlorogenic acid, and ferulic acid, according to HPLC chromatogram analysis. In this study, we used DFT to show that the constituent 3,4-dihydroxycinnamic acid has a higher chance of reacting with $Al(NO_3)_3$ and forming Al-MOF. This green synthesis is a fast, easy and inexpensive way of using no harmful organic matter. According to the results of FTIR analysis, the activation does not affect the organic ligand of Al-MOF. Furthermore, based on the BET results, it was revealed that the prepared Al-MOF sample seemed to have a higher surface area than the Al-MOF (MIL-100) synthesized with the terephthalic acid ligand. Based on the findings of the presented research, it can be concluded that the *S. hortensis* extract was successfully used in the preparation of Al-MOF. Furthermore, the MTT assay shows that Al-MOF has low cytotoxicity, good biocompatibility, and anti-cancer activity against MDA-MB-468 cell lines.

Declaration of Competing Interest

The authors declare that they have no competing interests.

The authors declare that they have no known competing financial interests or personal relationships that could have appeared to influence the work reported in this paper.

CRediT authorship contribution statement

Malihe Zeraati: Writing – original draft, Visualization, Writing – review & editing, Investigation, Data curation, Validation. **Vali Alizadeh:** Writing – review & editing. **Supat Chupradit:** Writing

– review & editing. **Narendra Pal Singh Chauhan:** Conceptualization, Writing – original draft, Writing – review & editing, Investigation, Visualization, Validation, Data curation, Supervision. **Ghasem Sargazi:** Conceptualization, Writing – original draft, Writing – review & editing, Investigation, Visualization, Validation, Data curation, Supervision.

References

[1] a) D. Chen, J. Zhao, P. Zhang, S. Dai, Polyhedron 162 (2019) 59–64; b) L. Paseta, G.g. Potier, S. Sorribas, J. Coronas, ACS Sustain Chem Eng 4 (2016) 3780–3785; c) G. Wu, J. Ma, S. Li, J. Guan, B. Jiang, L. Wang, J. Li, X. Wang, L. Chen, J. Colloid Interface Sci. 528 (2018) 360–371.

[2] A. Monguzzi, M. Ballabio, N. Yanai, N. Kimizuka, D. Fazzi, M. Campione, F. Meinardi, Highly fluorescent metal–organic-framework nanocomposites for photonic applications, Nano Lett. 18 (2017) 528–534.

[3] J. Canivet, A. Fateeva, Y. Guo, B. Coasne, D. Farrusseng, Water adsorption in MOFs: fundamentals and applications, Chem. Soc. Rev. 43 (2014) 5594–5617.

[4] S. H. Hashemi, M Kaykhaii, A. J Keikha, E Mirmoradzehi, G Sargazi, Application of response surface methodology for optimization of metal–organic framework based pipette-tip solid phase extraction of organic dyes from seawater and their determination with HPLC, BMC chem. 131 (1) (2019) 1–10.

[5] P. Valvekens, F. Vermoortele, D. De Vos, Metal–organic frameworks as catalysts: the role of metal active sites, Catal. Sci. Technol. 3 (2013) 1435–1445.

[6] Y.J. Jang, Y.E. Jung, G.W. Kim, C.Y. Lee, Y.D. Park, Metal–organic frameworks in a blended polythiophene hybrid film with surface-mediated vertical phase separation for the fabrication of a humidity sensor, RSC Adv. 9 (2019) 529–535.

[7] G Sargazi, D Afzali, A Mostafavi, H Kazemian, A novel composite derived from a metal organic framework immobilized within electrospun nanofibrous polymers: An efficient methane adsorbent, Appl. Organomet. Chem. 34 (3) (2020) e5448.

[8] I. Stassen, B. Bueken, H. Reinsch, J. Oudenhoven, D. Wouters, J. Hajek, V. Van Speybroeck, N. Stock, P. Vereecken, R. Van Schaijk, Towards metal–organic framework based field effect chemical sensors: UiO-66-NH 2 for nerve agent detection, Chemical science 7 (2016) 5827–5832.

[9] L Zhu, G Liang, C Guo, et al., A new strategy for the development of efficient impedimetric tobramycin aptasensors with metallo-covalent organic frameworks (MCOFs), Food Chem. 366 (2021) 130575.

[10] M. Gaab, N. Trukhan, S. Maurer, R. Gummaraju, U. Müller, The progression of Al-based metal-organic frameworks–From academic research to industrial production and applications, Microporous and mesoporous materials 157 (2012) 131–136.

[11] B. Khezri, M. Pumera, Metal–Organic Frameworks Based Nano/Micro/Millimeter-Sized Self-Propelled Autonomous Machines, Advanced Materials 31 (2019) 1806530.

[12] L.B. d. Freitas, D.M. Fernandes, S. Maia, A. Moniz, B.G. Mazziero, F. Steiner, Sources and doses of aluminum in experiments with rice in nutrient solution, Revista Brasileira de Engenharia Agrícola e Ambiental 23 (2019) 511–517.

[13] a) D. Liu, F. Dai, Z. Tang, Y. Liu, C. Liu, Mater. Res. Bull. 65 (2015) 287–292; b) L. Heinke, C. Wöll, Advanced Materials (2019) 1806324; c) J. Ma, S. Li, G. Wu, S. Wang, X. Guo, L. Wang, X. Wang, J. Li, L. Chen, J. Colloid Interface Sci. (2019).

[14] Z. Hu, E.M. Mahdi, Y. Peng, Y. Qian, B. Zhang, N. Yan, D. Yuan, J.-C. Tan, D. Zhao, Kinetically controlled synthesis of two-dimensional Zr/Hf metal–organic framework nanosheets via a modulated hydrothermal approach, Journal of Materials Chemistry A 5 (2017) 8954–8963.

[15] B.-J. Zhu, X.-Y. Yu, Y. Jia, F.-M. Peng, B. Sun, M.-Y. Zhang, T. Luo, J.-H. Liu, X.-J. Huang, Iron and 1, 3, 5-benzenetricarboxylic metal–organic coordination polymers prepared by solvothermal method and their application in efficient As (V) removal from aqueous solutions, J. Phys. Chem. C 116 (2012) 8601–8607.

[16] W. Xia, X. Zhang, L. Xu, Y. Wang, J. Lin, R. Zou, Facile and economical synthesis of metal–organic framework MIL-100 (Al) gels for high efficiency removal of microcystin-LR, RSC Adv. 3 (2013) 11007–11013.

[17] R.S. Pillai, H. Jobic, M.M. Koza, F. Nouar, C. Serre, G. Maurin, N.A. Ramsahye, Diffusion of carbon dioxide and nitrogen in the small-pore titanium bis (phosphonate) metal–organic framework MIL-91 (Ti): a combination of quasielastic neutron scattering measurements and molecular dynamics simulations, ChemPhysChem 18 (2017) 2739–2746.

[18] a) C. Kiener, U. Muller, M. Schubert, Organometallic Aluminum Fumarate Backbone Material, 2009. *Vol.* Google Patents; b) H.W.B. Teo, A. Chakraborty, Y. Kitagawa, S. Kayal, 2017 Int. J. Heat Mass Transf., 114 621–627.

[19] S. Kayal, A. Chakraborty, H.W.B. Teo, Green synthesis and characterization of aluminium fumarate metal-organic framework for heat transformation applications, Mater. Lett. 221 (2018) 165–167.

[20] a) Y. Zhou, Curr Nanosci 1 (2005) 35–42; b) J. Liu, F. Zhang, X. Zou, G. Yu, N. Zhao, S. Fan, G. Zhu, Chemical Communications 49 (2013) 7430–7432.

[21] B.H.W. Teo, Modulation and Green Synthesis of Metal Organic Frameworks For Higher Water Uptakes and kinetics: Adsorption Cooling Application, 2019 *Vol.*.

[22] A. Lozhkomoev, in: AIP Conference Proceedings, 2016.

[23] L. Chen, M. He, M. Zhang, Q. Sun, S. Zeng, H. Zhao, H. Yang, M. Liu, S. Ren, X. Meng, The Role of non-coding RNAs in colorectal cancer, with a focus on its autophagy, Pharmacol. Ther. (2021) 107868.

[24] H. Chunyan, et al., Recent progress in the research of Angelica sinensis (Oliv.) Diels polysaccharides: extraction, purification, structure and bioactivities, Chem. Biol. Technol. Agric. 8 (1) (2021) 1–14.

[25] a) T. Mihajilov-Krstev, D. Radnović, D. Kitić, B. Zlatković, M. Ristić, S. Branković, Open Life Sci 4 (2009) 411–416; b) I. Fierascu, C.E. Dinu-Pirvu, R.C. Fierascu, B.S. Velescu, V. Anuta, A. Ortan V.J.M. Jinga, 2018, 23, 2458.

[26] V. Hajhashemi, B. Zolfaghari, A. Yousefi, Antinociceptive and anti-inflammatory activities of Satureja hortensis seed essential oil, hydroalcoholic and polyphenolic extracts in animal models, Medical Principles and Practice 21 (2012) 178–182.

[27] I. Rasaee, M. Ghannadnia, S. Baghshahi, Biosynthesis of silver nanoparticles using leaf extract of Satureja hortensis treated with NaCl and its antibacterial properties, Microporous and Mesoporous Materials 264 (2018) 240–247.

[28] M. Couderchet, Plant Biochemistry, Academic Press, Chichester, New York, Weinheim, 2000 PM Dey, JB Harborne (Eds.)(1997), *Vol.* Urban & Fischer.

[29] Ji, Xiaolong, et al. Purification, Structure and Biological Activity of Pumpkin Polysaccharides: A Review. Food Reviews International (2021): 1-13.

[30] R.G. Parr, in: Density Functional Theory of Atoms and Molecules, Springer, 1980, pp. 5–15.

[31] a) P. Hohenberg, W. Kohn, Physical review 136 (1964) B864; b) M. Zeraati, K. Tahmasebi and A.J.J.o.N. Irannejad, 2020, 10, 660–670.

[32] a) A.Z. Thong, M.S. Shaffer, A.P. Horsfield, Sci. Rep. 8 (2018) 9120; b) M. Shakiba, G.R. Khayati, M. Zeraati, J Solgel Sci Technol (2019) 1–11.

[33] a) K. Momma, F. Izumi, J. Appl. Crystallogr. 44 (2011) 1272–1276; b) Z.X. Cai, Z.L. Wang, J. Kim, Y. Yamauchi, Advanced Materials 31 (2019) 1804903; c) S. Shafiee, H.A. Ahangar, A. Saffar, Carbohydr. Polym. 222 (2019) 114982.

[34] L. Lai, W.H. Green, Thermochemistry and Kinetics of Intermolecular Addition of Radicals to Toluene and Alkylaromatics, The Journal of Physical Chemistry A 123 (2019) 3176–3184.

[35] a) J. Wieme, K. Lejaeghere, G. Kresse, V. Van Speybroeck, Nat. Commun. 9 (2018) 4899; b) Y. Guan, Z. Teng, L. Mei, J. Zhang, Q. Wang, Y. Luo, J. Colloid Interface Sci. 533 (2019) 207–215.

[36] a) A.L. Mendieta-Jiménez, P. Carpio-Martínez, F. Cortés-Guzmán, R.M. Gómez-Espinosa, Chem. Phys. Lett. 693 (2018) 159–164; b) M. Frisch, Inc., Wallingford CT 2009.

[37] M. Alkasir, N. Samadi, Z. Sabouri, Z. Mardani, M. Khatami, M. Darroudi, (2020). Evaluation cytotoxicity effects of biosynthesized zinc oxide nanoparticles using aqueous Linum Usitatissimum extract and investigation of their photocatalytic activityackn. Inorganic Chemistry Communications, 119, 108066.

[38] O.K. Farha, J.T. Hupp, Rational design, synthesis, purification, and activation of metal−organic framework materials, Acc. Chem. Res. 43 (2010) 1166–1175.

[39] B. Hoskins, R. Robson, Design and construction of a new class of scaffolding–like materials comprising infinite polymeric frameworks of 3D-linked molecular rods. A reappraisal of the zinc cyanide and cadmium cyanide structures and the synthesis and structure of the diamond-related frameworks [N (CH3) 4][CuIZnII (CN) 4] and CuI [4, 4', 4'', 4'''-tetracyanotetraphenylmethane] BF4. xC6H5NO2, J. Am. Chem. Soc. 112 (1990) 1546–1554.

[40] J.E. Mondloch, O. Karagiaridi, O.K. Farha, J.T. Hupp, Activation of metal–organic framework materials, CrystEngComm 15 (2013) 9258–9264.

[41] P. Rallapalli, D. Patil, K. Prasanth, R.S. Somani, R. Jasra, H. Bajaj, An alternative activation method for the enhancement of methane storage capacity of nanoporous aluminium terephthalate, MIL-53 (Al), Journal of Porous Materials 17 (2010) 523–528.

[42] S.-H. Lo, C.-H. Chien, Y.-L. Lai, C.-C. Yang, J.J. Lee, D.S. Raja, C.-H. Lin, A mesoporous aluminium metal–organic framework with 3 nm open pores, Journal of Materials Chemistry A 1 (2013) 324–329.

[43] X. Qian, B. Yadian, R. Wu, Y. Long, K. Zhou, B. Zhu, Y. Huang, Structure stability of metal-organic framework MIL-53 (Al) in aqueous solutions, Int. J. Hydrogen Energy 38 (2013) 16710–16715.

[44] M. Valero, B. Zornoza, C. Téllez, J. Coronas, Mixed matrix membranes for gas separation by combination of silica MCM-41 and MOF NH2-MIL-53 (Al) in glassy polymers, Microporous and Mesoporous Materials 192 (2014) 23–28.

[45] H. Reinsch, R.S. Pillai, R. Siegel, J. Senker, A. Lieb, G. Maurin, N. Stock, Structure and properties of Al-MIL-53-ADP, a breathing MOF based on the aliphatic linker molecule adipic acid, Dalton Transactions 45 (2016) 4179–4186.

[46] V. Benoit, N. Chanut, R.S. Pillai, M. Benzaqui, I. Beurroies, S. Devautour-Vinot, C. Serre, N. Steunou, G. Maurin, P.L. Llewellyn, A promising metal–organic framework (MOF), MIL-96 (Al), for CO 2 separation under humid conditions, Journal of Materials Chemistry A 6 (2018) 2081–2090.

[47] N Firouzeh, V Malakootian, S. N Asadzadeh, M Khatami, M Makarem, Degradation of ciprofloxacin using ultrasound/ZnO/oxone process from aqueous solution-lab-scale analysis and optimization, BioNanoScience 11 (2) (2021) 306–313.

[48] L. Li, S. Xiang, S. Cao, J. Zhang, G. Ouyang, L. Chen, C.-Y. Su, A synthetic route to ultralight hierarchically micro/mesoporous Al (III)-carboxylate metal-organic aerogels, Nat. Commun. 4 (2013) 1774.

[49] S.M. Mirsoleimani-azizi, P. Setoodeh, S. Zeinali, M.R. Rahimpour, Tetracycline antibiotic removal from aqueous solutions by MOF-5: Adsorption isotherm, kinetic and thermodynamic studies, Journal of environmental chemical engineering 6 (2018) 6118–6130.

[50] Q. Zhang, Y. Ding, S. Gu, S. Zhu, X. Zhou, Y. Ding, Identification of changes in volatile compounds in dry-cured fish during storage using HS-GC-IMS, Food Research International 137 (2020) 109339.

[51] a) Y. Hu, Y. Chen, Y. Liu, W. Li, M. Zhu, P. Hu, H. Jin, Y. Li, Microporous and Mesoporous Materials 270 (2018) 67–74; b) M. Mihaylov, S. Andonova, K. Chakarova, A. Vimont, E. Ivanova, N. Drenchev, K. Hadjiivanov, Physical Chemistry Chemical Physics 17 (2015) 24304–24314; c) B. Seoane, C. Téllez, J. Coronas, C. Staudt, Sep. Purif. Technol. 111 (2013) 72–81.

[52] D. Saha, R. Zacharia, L. Lafi, D. Cossement, R. Chahine, Synthesis, characterization and hydrogen adsorption properties of metal–organic framework Al-TCBPB, Int. J. Hydrogen Energy 37 (2012) 5100–5107.
[53] Z. Nowroozi-Nejad, B. Bahramian, S. Hosseinkhani, A fast and efficient stabilization of firefly luciferase on MIL-53 (Al) via surface adsorption mechanism, Research on Chemical Intermediates 45 (2019) 2489–2501.
[54] C. Volkringer, D. Popov, T. Loiseau, G. Férey, M. Burghammer, C. Riekel, M. Haouas, F.J.C.o.M. Taulelle, 2009, 21, 5695–5697.
[55] D. Wang, H. Wu, W.Q. Lim, S.Z.F. Phua, P. Xu, Q. Chen, Z. Guo, Y. Zhao, A mesoporous nanoenzyme derived from metal–organic frameworks with endogenous oxygen generation to alleviate tumor hypoxia for significantly enhanced photodynamic therapy, Advanced Materials (2019) 1901893.
[56] E. Rahmani, M. Rahmani, Al-based MIL-53 metal organic framework (MOF) as the new catalyst for Friedel–Crafts alkylation of benzene, Ind. Eng. Chem. Res. 57 (2017) 169–178.
[57] X. Ji, C. Hou, Y. Gao, Y. Xue, Y. Yan, X. Guo, Metagenomic analysis of gut microbiota modulatory effects of jujube (Ziziphus jujuba Mill.) polysaccharides in a colorectal cancer mouse model, Food Funct 11 (2020) 163–173.
[58] a) E. Tuncer, S. Unver-Saraydin, B. Tepe, S. Karadayi, H. Ozer, M. Sen, K. Karadayi, D. Inan, S. Elagoz, Z. Polat, J BUON 18 (2013) 77–85; b) A.R. Chowdhuri, D. Laha, S. Chandra, P. Karmakar, S.K. Sahu, Chem. Eng. J. 319 (2017) 200–211; c) S. Pathak, M.K. Ghosh, M. Mandal, V. Mandal, A. Bhattacharyya, T.K. Ghorai, New J. Chem. (2019) 43; d) A.K. Ebrahimi, I. Sheikhshoaie, M. Mehran, J. Mol. Liq. 240 (2017) 803–809.